Chemical Science

ROYAL SOCIETY OF CHEMISTRY

EDGE ARTICLE

View Article Online
View Journal | View Issue



Cite this: *Chem. Sci.*, 2022, **13**, 13393

All publication charges for this article have been paid for by the Royal Society of Chemistry

Received 20th September 2022
Accepted 26th October 2022

DOI: 10.1039/d2sc05231h

rsc.li/chemical-science



# Electro-optic crosslinkable chromophores with ultrahigh electro-optic coefficients and long-term stability†

Ziying Zeng,[a] Jianhua Liu,*[b] Tongyu Luo,[a] Zhibei Li,[a] Juanfei Liao,[a] Weijun Zhang,[a] Lian Zhang[a] and Fenggang Liu *[a]

The development of organic electro-optic materials with ultrahigh electro-optic coefficients and high long-term alignment stability is the most challenging topic in this field. Next-generation crosslinkable nonlinear optical chromophore molecular glasses were developed to address this problem. A highly stable EO system including crosslinkable binary chromophores QLD1 and QLD2 or crosslinkable single chromophore QLD3 and multichromophore QLD4 with large hyperpolarizability was synthesized using tetrahydroquinoline as the donor. When the temperature continues to rise after poling, the chromophores modified with anthracene and acrylate can undergo Diels–Alder crosslinking reaction to fix the oriented chromophores through chemical bonds. After crosslinking, the QLD1/QLD2 and QLD2/QLD4 films achieved very high maximum $r_{33}$ values of 327 and 373 pm $V^{-1}$, respectively, which are the highest values reported for crosslinkable chromophore systems. After Diels–Alder cycloaddition, the glass transition temperature of the EO film increased by ~90 °C to 185 °C, which is higher than for any other pure chromophore films. After being annealed at 85 °C, 99.63% of the initial $r_{33}$ value could be maintained for over 500 h. The ultrahigh electro-optic activity and high long-term alignment stability of these materials showed new breakthroughs in organic EO materials for practical device explorations.

## 1 Introduction

With the global spread of COVID-19, more work has to be done online, which has aroused people's desire for faster broadband services. Moving forward to the next-generation network and 5G will help to solve this problem. Our entire communication network now relies heavily on optical communication technology. Our backbone network, optical broadband and 5g are all inseparable from the support of optical communication technology. An electro-optic modulator is a key functional device that loads electronic signals onto optical carriers. Electro-optic material is the core component of an electro-optic modulator.[1,2] At present, most of the materials in commercial devices are inorganic materials, such as lithium niobate ($LiNbO_3$) and other inorganic crystal materials.[3]

Organic nonlinear optical materials have the advantages of high electro-optic coefficient, fast response speed and good processability and integration, having great applications in high-speed information transmission,[4] optical communication,[5] optical information storage, terahertz technology,[6] and other fields.[7,8] Recently, CLD-type organic second-order nonlinear chromophores have been used to prepare 500 GHz electro-optic modulators,[9,10] terahertz field detectors,[11,12] plasmonic devices[13–15] and other optoelectronic devices.[16,17] All of these indicate that organic second-order nonlinear chromophores have broad practical prospects.

However, the practical application of organic electro-optic chromophores still faces many challenges. How to obtain organic electro-optic chromophores with a large electro-optic coefficient ($r_{33}$ value), photothermal stability and polarization orientation stability is still a problem to be solved.[18,19] In order to show the electro-optic activity, the chromophore molecules need to be polarized under the electric field and exhibit a non-centrosymmetric arrangement. However, the chromophore molecules usually have large dipole moments, and the electrostatic interaction between the molecules will hinder the ordered arrangement, thus reducing the macroscopic electro-optic coefficient.[20,21] It has been reported in the literature that introducing branching groups to the donor, electron bridge or acceptor of a chromophore can weaken the dipole–dipole interaction, allowing a higher electro-optic coefficient to be obtained.[22,23] Researchers also put forward the concept of a dendrimer,[24,25] which connects multiple chromophore molecules together through chemical bonds to form a dendritic structure,[26,27] and further weakens the electrostatic interaction between molecules.

[a]*School of Chemistry and Chemical Engineering, Guangzhou University, Guangzhou 510006, P. R. China. E-mail: liufg6@gzhu.edu.cn*

[b]*Huawei Technologies, Bantian Industrial Base, Shenzhen 518129, P. R. China. E-mail: liujianhua.liu@huawei.com*

† Electronic supplementary information (ESI) available. See DOI: https://doi.org/10.1039/d2sc05231h

Many branched chromophores with excellent properties have been designed to weaken the dipole–dipole interaction and the electro-optic coefficient has been greatly improved, exceeding 300 pm $V^{-1}$.[28] However, compared with polymers, the glass transition temperature of small chromophore molecules is lower, and the polarization orientation stability of organic electro-optic materials has long been a technical bottleneck in this field. At high temperature, under the action of an electric field the ordered arrangement of chromophore molecules will degenerate into disordered isotropic arrangement due to electrostatic interaction, and the electro-optic coefficient will also decline. The main-chain or side-chain polymers have high $T_g$, but their low electro-optic coefficients limit their application.[29] New crosslinked electro-optic materials have started to appear, and have become the most promising new electro-optic materials for achieving a high electro-optic coefficient and high orientation stability.[30] After polarization orientation, a crosslinking reaction takes place between molecules, forming a chromophore network in the form of chemical bonds, fixing the oriented chromophore molecules, and greatly improving the stability of the poling orientation of the material.

However, there are few reports on crosslinked electro-optic materials, and many of them are in exploratory research.[31–37] At present, crosslinked electro-optic materials still have the following problems: the crosslinked objects are mainly chromophores and polymers/small molecules.[38] Because of the presence of polymer or small-molecule crosslinking agents, the chromophore content is low (usually less than 25 wt%). Although the introduction of binary chromophores can increase the chromophore content, it significantly reduces the glass transition temperature.[39] We abandoned the traditional polymer crosslinking system and developed a new type of binary crosslinked molecular glass (neat EO materials) called HLD1/HLD2, as we previously reported in the literature and as shown in Fig. S16, ESI.† [40] The chromophore content in the electro-optic film is as high as 100 wt% without any small-molecule or polymer crosslinkers, which is beneficial to the improvement of the electro-optic coefficient. Moreover, after crosslinking, the glass transition temperature of the chromophore is also greatly improved. This is a material with a high electro-optic coefficient and stability. However, chromophores HLD1/HLD2 still have much room for improvement. For example, the first-order hyperpolarizability of chromophores HLD1/HLD2 is still not large enough, and their glass transition temperature needs to be improved. We therefore developed the next generation of crosslinked molecular glasses, QLD1–QLD4, as shown in Fig. 1. We used tetrahydroquinoline as the donor chromophore, which makes the first-order hyperpolarizability of the QLD chromophore series about ~15% higher than that of the HLD series, which is promising for obtaining a larger electro-optic coefficient. At the same time, due to the introduction of new donors and new configurations, the glass transition temperature of the chromophores has also increased by 10–40 °C. In addition, a crosslinkable single-component electro-optic material, QLD3, and a crosslinkable multi-chromophore, QLD4, were proposed for the first time. The QLD series materials have electro-optical coefficients larger than 300 pm $V^{-1}$ and glass transition temperatures of more than 185 °C, showing excellent performance.

## 2 Results and discussion

### 2.1 Thermal stability

In order to understand the decomposition of QLD1–4 at high temperatures, the four chromophores were tested using

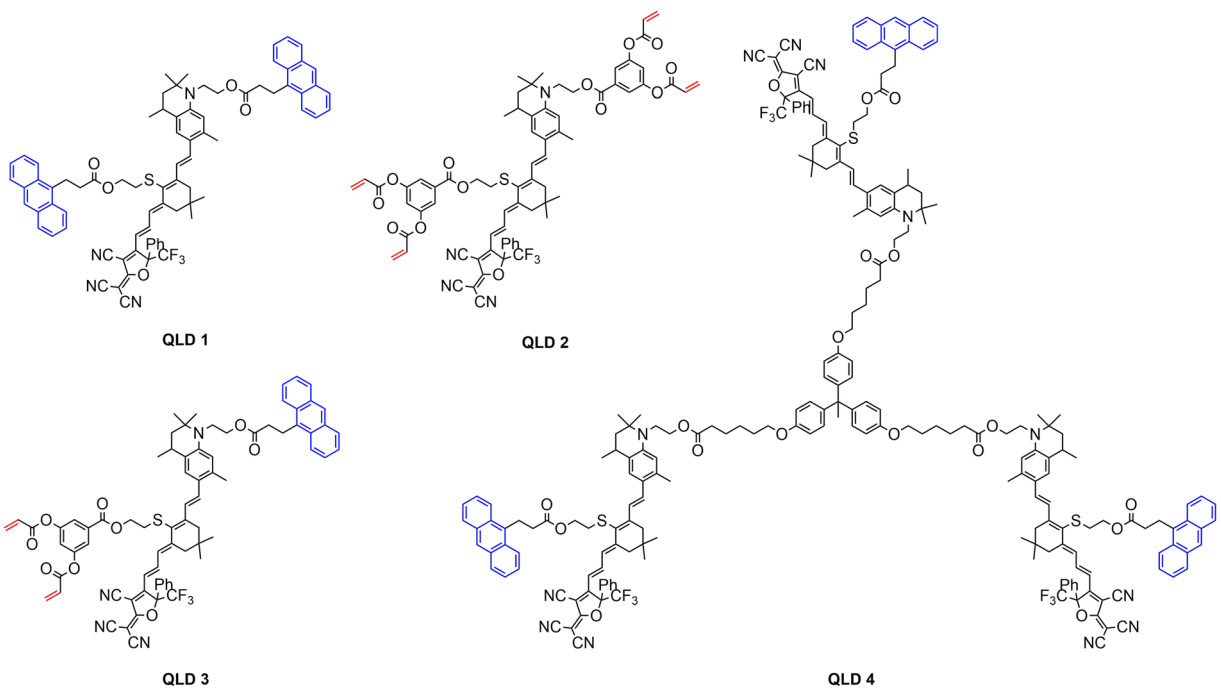


Fig. 1 Chemical structure for chromophores QLD1–4.

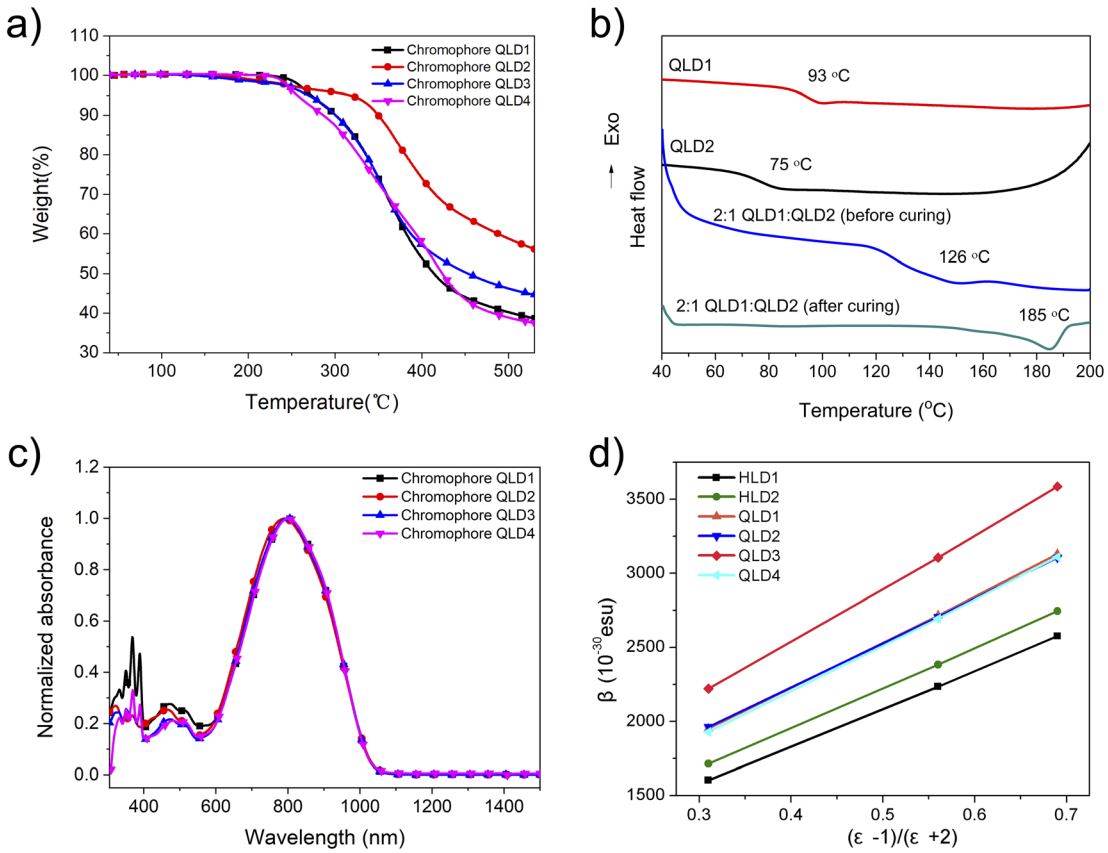


Fig. 2 (a) TGA curves of chromophores QLD1–4. (b) DSC curves of chromophores QLD1 and QLD2. (c) UV-vis absorption spectra of chromophores QLD1–4 in chloroform. (d) Hyperpolarizability in toluene, chloroform and tetrahydrofuran solution for chromophores HLD1, HLD2, and QLD1–4 calculated by DFT (M062X/6-31+G(d)).

a thermogravimetric analyser (TGA) under nitrogen at a heating rate of 10 °C $min^{-1}$ and the obtained results are shown in Fig. 2a and Table 1. All four chromophores exhibited good thermal stability, with all of them decomposing at temperatures ($T_d$, 5% weight loss) above 250 °C (257–317 °C), which facilitates the exploration of polarization processes and the fabrication of EO devices. Among the four synthesized chromophores, chromophore QLD2 had the highest decomposition temperature ($T_d$, 317 °C), followed by chromophore QLD1 ($T_d$, 273 °C), chromophore QLD3 ($T_d$, 270 °C) and chromophore QLD4 ($T_d$, 257 °C).

The glass transition temperature ($T_g$) is an important indicator for chromophores, affecting the poling temperature and long-term alignment stability of the material. The glass transition temperature is very important for the stability of the electro-optic coefficient. When the temperature exceeds the glass transition temperature, the chromophore molecules with polarization orientation under the electric field can easily return to the isotropic arrangement, thus losing the electro-optic coefficient. For pure chromophore films, the glass transition temperature is usually less than 120 °C.[41,42] The occurrence of a crosslinking reaction helps to improve the glass transition temperature, which was confirmed by the test results.

Table 1 Thermal and optical properties data of the chromophores

| Compound | $T_d$ (°C) | $\lambda_{max}{}^a$ (nm) | $\lambda_{max}{}^b$ (nm) | $\Delta\lambda^c$ (nm) | $T_g$ (°C) |
|---|---|---|---|---|---|
| QLD1 | 273 | 800 | 737 | 63 | 93 |
| QLD2 | 317 | 790 | 734 | 56 | 75 |
| QLD3 | 270 | 798 | 721 | 77 | 74 |
| QLD4 | 257 | 801 | 721 | 80 | 122 |

[a] Measured in chloroform. [b] Measured in dioxane. [c] The difference between $\lambda_{max}{}^a$ and $\lambda_{max}{}^b$.

The glass transition temperature ($T_g$) of the chromophores was measured using differential scanning calorimetry (DSC), as shown in Fig. 2b and S13–15, ESI.† The glass transition temperatures of the chromophores QLD1–4 were 93 °C, 75 °C, 74 °C and 122 °C, respectively. The glass transition temperature of chromophore QLD1 is 20 °C higher than that of HLD1, which also explains why the crosslinked QLD1/QLD2 has a higher glass transition temperature than HLD1/HLD2. The glass transition temperature of chromophore HLD4 was further increased to 120 °C due to the larger molecular weight of the multi-chromophore configuration.

Then, we doped the chromophores QLD1 and QLD2 in a 2 : 1 mass ratio, and during the heating process (150 °C for 30 min), the anthracene group of QLD1 and the acrylate group of QLD2 would crosslink and the small molecules would thus become

polymers. After crosslinking, the glass transition temperature of 2 : 1 QLD1 : QLD2 was increased to 185 °C; the anthracene group of QLD3 reacts with the acrylate group after crosslinking and the glass transition temperature was measured to be 184 °C. The glass transition temperatures of 2 : 1 QLD1/QLD2 and QLD3 after crosslinking were similar, which may indicate that the crosslinking reaction only occurs between one anthracene group and one double bond of acrylate owing to the steric hindrance. The glass transition temperatures of the 2 : 1 QLD1/QLD2 and QLD3 chromophores after crosslinking exceed 180 °C, placing them among the highest reported glass transition temperatures for pure chromophores.[43]

### 2.2 Optical properties

In order to compare the effect of different electron donors on the charge transfer ability of the chromophores, the UV-vis absorption spectra of the four chromophores were tested in different solvents and films with different dielectric constants. As shown in Fig. 2c and S11, ESI,† the maximum absorption wavelengths of the chromophores QLD1–4 in chloroform are 800 nm, 790 nm, 798 nm and 801 nm, respectively. Compared to the chromophores HLD1 and HLD2 (745 nm and 742 nm), which are based on common aniline derivatives, the maximum absorption wavelength of the chromophores QLD1–4 was redshifted by about 50 nm. The six-membered ring structure on the tetrahydroquinoline donor effectively enhances its electron donor ability, reduces the molecular energy range, and thus causes a red shift. The larger UV absorption wavelengths indicate that the QLD series chromophores have greater first-order hyperpolarizability than HLD, which is consistent with the later theoretical calculation results.

The solvatochromic behavior of the four chromophores was also studied in six different polar solvents, as shown in Fig. S11, ESI.† The solvent-dependent spectral behavior of the chromophores was similar to that of tetrahydroquinolinyl-based CLD-type chromophores, which suggests that the chromophores QLD1–4 could be polarized quite close to the cyanine limit in the most polar solvents due to the use of stronger tetrahydroquinoline-based electron donors.[30] The thin film $\lambda_{max}$ values ranged from 790 to 801 nm for QLD1–4, 2 : 1 QLD1/QLD2 and 3 : 4 QLD2/QLD4. In addition to the main absorption peak, there is also a long-wavelength shoulder of UV absorption in the film, which was attributed to the formation of aggregates at higher chromophore concentrations. This phenomenon is also common in films with similar chromophores such as HLD1–2.[40,44]

To determine the effect of crosslinking, UV absorption spectra were determined in films of QLD1 alone and QLD2 alone; in an uncrosslinked 2 : 1 blend of QLD1 and QLD2; and in a crosslinked 2 : 1 blend of QLD1 and QLD2. QLD3 was tested in films before and after crosslinking alone. QLD4 was crosslinked with QLD2 and tested similarly to QLD1 and QLD2. The film of 2 : 1 QLD1/QLD2 showed an absorption maximum at 782 nm that was blue-shifted to 761 nm after baking at 150 °C under vacuum for 30 min to allow the crosslinking reaction to occur. Similarly, chromophores QLD3 and QLD2/QLD4 also have blue shifts of 25 and 24 nm, respectively, after heating and crosslinking, as shown in Fig. S12, ESI.† The occurrence of a crosslinking reaction can also be confirmed by the UV absorption of the film before and after heating. The anthracene functional group has an absorption peak between 325 and 400 nm. Upon heating, the intensity of the anthracenyl absorption bands located at around 350, 370, and 390 nm decreased significantly, thus proving that the crosslinking reaction between anthracene and acrylate does take place. At the same time, it is worth noting that when heated at 150 °C for 30 minutes, the main absorption peak of the chromophore did not decrease, which indicates that the crosslinking reaction can effectively enhance the stability of the chromophore.

### 2.3 Theoretical calculations

In order to compare the microscopic nonlinearities, charge transfer and steric configurations of the different chromophores, structural optimisation and theoretical calculation of the first-order hyperpolarizability were carried out for chromophores QLD1–4. For the stereo configuration, the theoretical calculations were performed using the Gaussian 09 software package, the cam-B3LYP method of the density functional method (DFT) combined with the 6-31g(d,p) basis group.[45,46] For the calculations, the chromophores were optimised assuming that all molecules were in the trans configuration and we calculated the ground and excited state energy levels, dipole moment ($\mu$), electron cloud density and microscopic first-order hyperpolarizability $\beta$ for the chromophores. The charge transfer interactions within the chromophores can be calculated from the energy level differences between the HOMO and LUMO molecular orbitals.

DFT calculations were used to determine the HOMO–LUMO energy level difference ($\Delta E$) for the chromophores QLD1–4 with values of 1.96 eV, 1.91 eV, 1.97 eV and 1.97 eV, respectively, as shown in Table 2. As the energy level difference ($\Delta E$) within a series of chromophores and their analogues increases, a blue shift of $\lambda_{max}$ is observed, which corresponds to the findings observed in the UV-vis spectral analysis. Among these four chromophores, the $\beta$ values did not show significant differences owing to the consistent structure of the chromophore bodies. We also calculated the first-order hyperpolarizabilities of the classical crosslinkable chromophores HLD1–2 as a comparison. According to the calculation results, the first-order hyperpolarizability of chromophores QLD1–4 was higher than those of HLD1–2 due to a narrow energy level difference between the

Table 2 Summary of UV-vis and DFT data

| Compound | $\lambda_{max}$ (nm) | $\Delta E$ (DFT)[a] (eV) | $\beta_{tot}$[b] ($10^{-30}$ esu) | $\mu$[c] (D) |
|---|---|---|---|---|
| QLD1 | 800 | 1.96 | 1130 | 24.5 |
| QLD2 | 790 | 1.91 | 1155 | 23.3 |
| QLD3 | 798 | 1.97 | 1177 | 24.8 |
| QLD4 | 801 | 1.97 | 1109 | 24.3 |
| HLD1 | 745 | 2.02 | 969 | 23.5 |
| HLD2 | 742 | 2.02 | 1027 | 23.6 |

[a] Calculated from DFT calculations. [b] The first-order hyperpolarizability in vacuum calculated from DFT calculations. [c] The total dipole moment.

HOMO and LUMO. This proves that introducing tetrahydroquinoline into the donor of a crosslinkable chromophore can significantly improve the first-order hyperpolarizability. DFT calculations were also performed at the M062X/6-31+G(d) level of theory in implicit solvent (PCM) environments in different solvent, such as THF, chloroform and toluene, to assess the effects of solvent on the dipole moments and hyperpolarizability, as shown in Fig. 2d and Table S1, ESI.† The chromophore achieved the maximum first-order hyperpolarizability in tetrahydrofuran, rather than in chloroform. The first-order hyperpolarizability of chromophores QLD1–4 in solvent was also higher than those of HLD1–2.

### 2.4 Testing of electro-optical coefficients

In order to test the electro-optic coefficients of the binary crosslinked molecular glassed, we prepared pure chromophore films from the chromophores, and then polarized them under different conditions to test the electro-optic coefficients of the uncrosslinked and crosslinked molecular glasses. The preparation steps before polarization are as follows: the neat chromophores were ultrasonicated for 15 minutes, dissolved in freshly distilled dibromomethane and then filtered through a syringe with 0.2 μm PTFE filter material. The filtered chromophore solution was spin-coated with indium oxide (ITO) glass substrate. The films were heated for 12 h in a vacuum at 50 °C (for drying) or 65 °C (for pre-crosslinking) to ensure removal of residual solvents or for the pre-crosslinking process.[40] The contact polarization process takes place at the appropriate temperature to polarize as many molecules as possible. The electro-optic coefficient ($r_{33}$) was tested using the Teng-Man simple reflection method at the wavelength of 1310 nm.[47] A benzocyclobutene (BCB) charge injection barrier

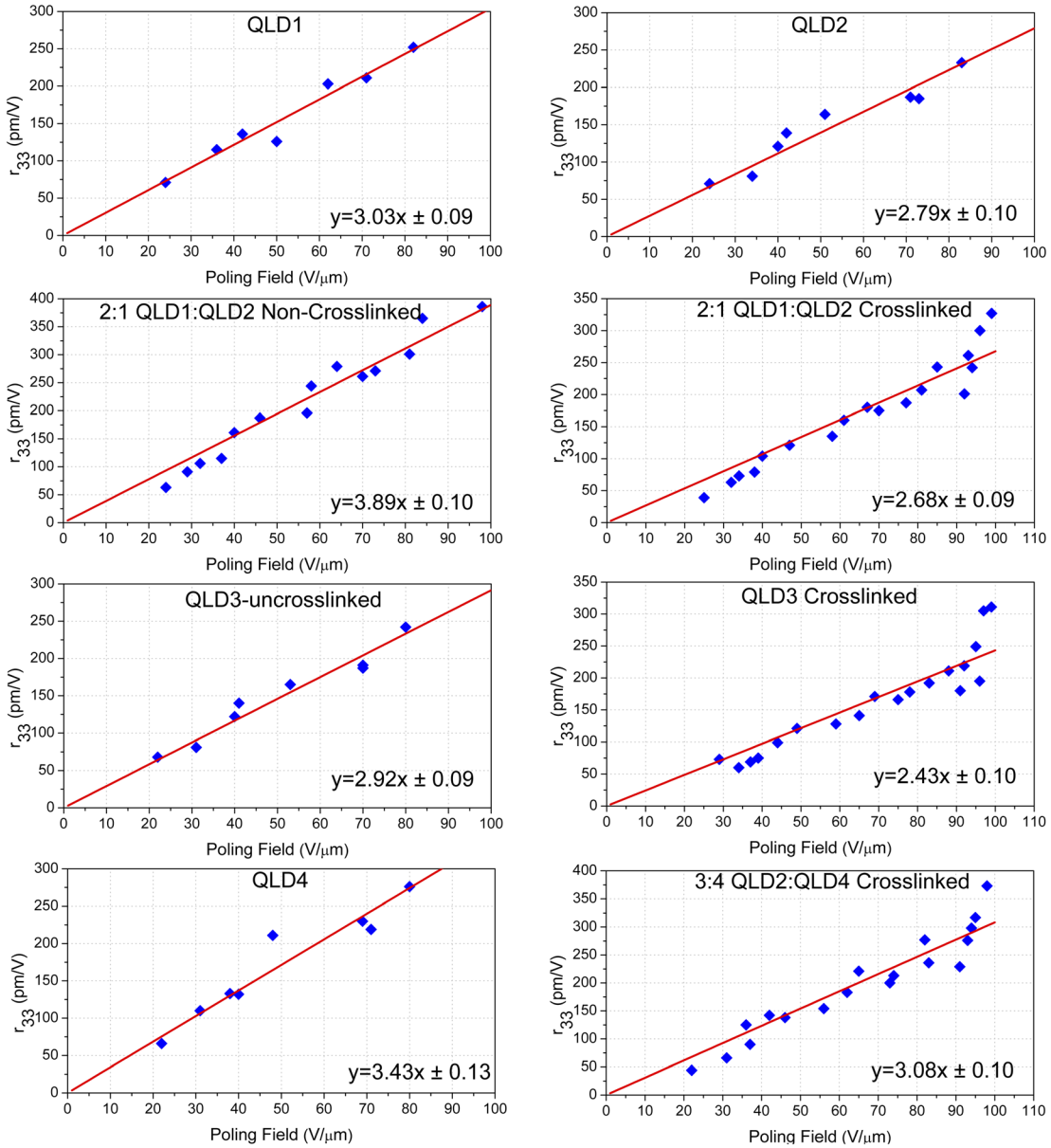


Fig. 3 Poling curve plots of $r_{33}$ *vs.* poling field.

Table 3 Electric field poling data for EO chromophores in bulk devices

| Compound | $\rho_N$ ($\times 10^{20}$ molecules per cm$^3$)[a] | Poling temp. (°C) | $r_{33}$ /E$_p$ (nm$^2$ V$^{-2}$)[b] | $r_{33}$ /(E$_p\rho_N$)[c] | Max. $r_{33}$ (pm V$^{-1}$) |
|---|---|---|---|---|---|
| QLD1 | 4.84 | 99 | 3.03 ± 0.09 | 0.63 ± 0.02 | 252 |
| QLD2 | 4.74 | 81 | 2.79 ± 0.10 | 0.59 ± 0.02 | 233 |
| QLD3 | 4.79 | 80 | 2.92 ± 0.09 | 0.61 ± 0.02 | 242 |
| QLD4 | 4.97 | 127 | 3.43 ± 0.13 | 0.69 ± 0.03 | 276 |
| QLD1 : QLD2 | 4.81 | 95 | 3.89 ± 0.10 | 0.81 ± 0.02 | 386 |
| 2 : 1 QLD1/QLD2 (crosslinked) | 4.81 | 100–160 | 2.68 ± 0.09 | 0.56 ± 0.02 | 327 |
| QLD3 (crosslinked) | 4.79 | 100–160 | 2.43 ± 0.10 | 0.51 ± 0.02 | 311 |
| 3 : 4 QLD2/QLD4 (crosslinked) | 4.87 | 100–160 | 3.08 ± 0.10 | 0.63 ± 0.02 | 373 |

[a] Number density (assumes mass density of 1 g cm$^{-3}$). [b] Average from multiple poling experiments. [c] Poling efficiency per number density (nm$^2$ V$^{-2}$/($10^{20}$ molecules per cm$^3$)).

layer was used between the ITO and the EO material for some devices.[44,48]

We first tested the macro electro-optical performance of the chromophores without crosslinking. The polarization process is a conventional poling process, and the poling temperature is 5–10 °C higher than the glass transition temperature of the chromophore. The average poling efficiencies ($r_{33}$/poling field or $r_{33}$/Ep) of QLD1 and QLD2 were 3.03 ± 0.09 and 2.79 ± 0.10 nm$^2$ V$^{-2}$, respectively, as shown in Fig. 3 and Table 3. These values were larger than those for chromophores HLD1 and HLD2 due to the larger hyperpolarizability. Because the conjugated structure of the chromophore molecules has not changed, chromophore QLD3 shows a poling efficiency similar to those of QLD1 and QLD2. The mutichromophore QLD4 with dendritic structure shows greater polarization efficiency than QLD3. This is because chromophores are separated by chemical bonds, which reduces the dipole–dipole interaction between molecules and improves the efficiency of polarization. Because it is a pure chromophore electro-optic film, too high voltage cannot be loaded on the film (limited to about 80 V μm$^{-1}$), so the electro-optic coefficient cannot continue to increase with the increase of voltage.

We then tested the polarization efficiency and electro-optic coefficient in the crosslinked state. The films of 2 : 1 QLD1/QLD2 and QLD3 itself were dried *in vacuo* at 65 °C for 12 h for precrosslinking to allow higher voltage loading. The poling process is also different from the normal chromophore poling process. We adopted a step poling method to prevent the membrane from cracking. The specific poling procedure was as follows: the desired poling field was applied, then the sample was heated to 130 °C at 10 °C min$^{-1}$ and held for 10 min, heated to 140 °C and held for 10 min, then heated to 150 °C and held for 10 min, and then cooled to room temperature. With the progress of the crosslinking reaction, the allowable loading voltage increased to ~100 V μm$^{-1}$, but too high voltage will break the gold electrode.

The average poling efficiencies of QLD1/QLD2 (2 : 1) and QLD3 after poling/crosslinking were 2.68 ± 0.09 and 2.43 ± 0.10 nm$^2$ V$^{-2}$, respectively, as shown in Fig. 4a. Large polarizability results in a large maximum $r_{33}$ value. The electro-optic coefficients of crosslinked QLD1/QLD2 (2 : 1) and QLD3 were as high as 327 pm V$^{-1}$ and 311 pm V$^{-1}$, respectively. The larger first-order hyperpolarizability of the QLD series of chromophores creates a larger electro-optic coefficient. For binary chromophores QLD1 and QLD2 without crosslinking, the electro-optic coefficient is as high as 327 pm V$^{-1}$, which is higher than the value of QLD1/QLD2 after crosslinking. This is also easy to understand: the crosslinking process will hinder the polarization of chromophores to a certain extent, resulting in lower poling efficiency. Owing to the participation of

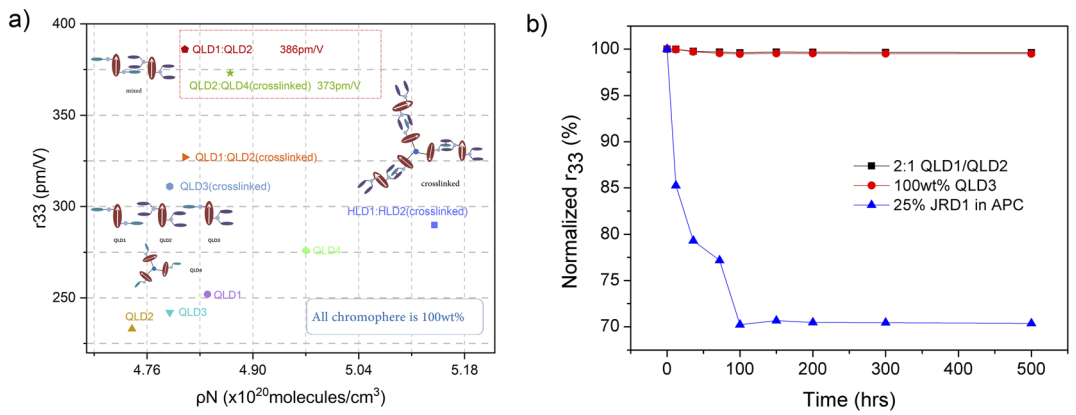


Fig. 4 (a) The EO coefficients of chromophores QLD1–4 and their mixtures as a function of N. (b) Temporal stability of the poled films QLD1/QLD2, QLD3 and JRD1/APC at the temperature of 85 °C in vacuum.

mutichromophore dendrimers, the electro-optic coefficient of crosslinked QLD2/QLD4 was further increased to 373 pm $V^{-1}$. These values were the highest reported for crosslinked organic electro-optic materials.

For practical device applications, electro-optic materials must withstand long-term stability tests at high temperatures, which is called alignment stability, and the results of the stability tests are shown in Fig. 4b. Devices that have been polarized and tested for electro-optic coefficient were placed in a vacuum drying oven at 85 °C and taken out at regular intervals to test the electro-optic coefficient. After testing, the poled and crosslinked electro-optic films 2 : 1 QLD1/QLD2 and QLD3 can still maintain the original electro-optic coefficient of more than 99.63% after being placed at 85 °C for 500 h.

## 3 Comparison and future prospects of different crosslinking systems

There are four types of crosslinked organic electro-optical materials. As shown in Fig. 5a and S20, ESI,† the most common type is polymer crosslinked materials, Although the electro-optical coefficient (<150 pm $V^{-1}$) of polymer-type crosslinked materials is lower due to the insufficient chromophore content, the higher glass transition temperature (as high as 215 °C or more) was an advantage. We can use polymers to improve the glass transition temperature of crosslinked systems. Binary crosslinkable chromophore is the second type of recently developed crosslinked electro-optic material, as shown in Fig. 5b. Represented by the HLD and QLD series, the 100% chromophore content and the effective occurrence of a crosslinking reaction enable the system to achieve a balance between the electro-optical coefficient (~300 pm $V^{-1}$) and the glass transition temperature (~170–185 °C). Such materials have been widely used in advanced optoelectronic devices and are expected to be commercially applied.[4] However, two-component materials may cause complexity in the mixing process, and the glass transition temperature still has room for improvement. As shown in Fig. 5c, a single-component crosslinkable electro-optic material QLD3 was proposed for the first time. This type of material has a similar electro-optical coefficient and glass transition temperature to the binary crosslinkable material without considering the different proportions and properties of the two components. It is worth further study to optimise the performance of single-component crosslinkable electro-optic chromophores. The fourth type is multi-chromophore crosslinked material represented by QLD4, as shown in Fig. 5d. Benefiting from the weakening of intermolecular electrostatic interactions, the electro-optical coefficient of chromophore was further improved, and with the increase of molecular weight, the glass transition temperature is also expected to further increase. However, the complexity of the synthesis steps of this material was a major disadvantage.

In order to meet the strict requirements of practicality and commercialization, the design of crosslinked organic electro-optic materials may be improved from two aspects: Firstly,

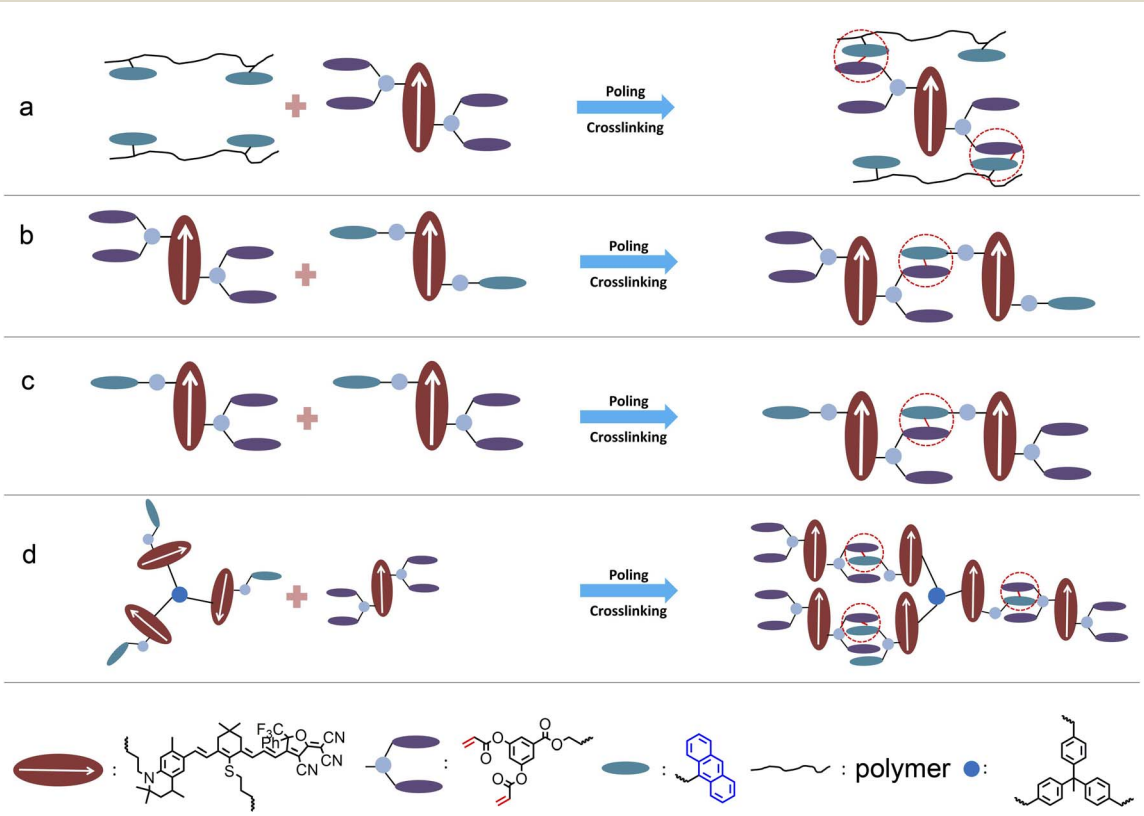


Fig. 5 Artistic comparison of four crosslinking systems: (a) crosslinkable polymer materials. (b) Crosslinkable binary chromophore. (c) Crosslinkable single chromophore. (d) Crosslinkable mutichromophore.

more efficient synthesis is more conducive to large-scale industrial production. At present, the synthesis of the tetrahydroquinoline donor is relatively complex. One solution is to find a new donor that is more conducive to synthesis or that can be purchased, but it must have similar or stronger donor strength to tetrahydroquinoline, such as aminosalicylaldehyde derivatives. Another solution is to adopt a more simplified chromophore synthesis scheme, such as the three-step synthesis method reported in the literature.[18] On the other hand, the glass transition temperature of the material also needs to be improved, preferably to more than 200 °C. Proper introduction of a small amount of polymer could help to increase the glass transition temperature without significantly reducing the chromophore content.

# 4 Conclusion

In order to develop organic second-order nonlinear optical materials with large electro-optic coefficients and good stability, and make them meet the strict requirements of commercial and practical devices, we developed a new generation of crosslinkable nonlinear optical chromophore molecular glasses including crosslinkable binary chromophores QLD1 and QLD2, crosslinkable single chromophore QLD3 and multichromophore QLD4. The driven EO chromophores were based on tetrahydroquinoline donors, isophorone-derived bridges and a $CF_3$-TCF acceptor. The functionalized groups anthracene and acrylate were modified on the donor and electron bridge of chromophores QLD1 and QLD2, respectively. The donor and bridge of chromophore QLD3 are respectively connected with anthracene and acrylate groups to form a self-crosslinking configuration. In addition, we synthesized multi-chromophore QLD4 by linking three crosslinkable chromophores together with chemical bonds. Compared with the classic highly stable binary crosslinkable chromophores HLD1 and HLD2, chromophores QLD1–4 adopt a stronger tetrahydroquinoline donor. This gives chromophores QLD1–4 greater first-order hyperpolarizability and higher glass transition temperatures. The 2 : 1 QLD1/QLD2 film achieved a very high maximum $r_{33}$ value of 327 pm $V^{-1}$ after crosslinking, which is the highest among crosslinkable chromophore systems. After Diels–Alder cycloaddition, the glass transition temperature of the EO film increased by ~90 °C to 185 °C, which is higher than for any other pure chromophore films. After being annealed at 85 °C, 99.63% of the initial $r_{33}$ value could be maintained for over 500 h. Ultrahigh electro-optic activity and high long-term alignment stability of these materials showed new breakthroughs in organic EO materials for practical device exploration.

# Data availability

All experimental procedures and compound characterization can be found in the ESI.†

# Author contributions

Z. Zeng, J. Liu and F. Liu conceived and developed the idea of the project. Z. Zeng and T. Luo carried out the synthesis of the chromophores. Z. Li and J. Liao carried out the TGA, DSC, UV-vis and electro-optical coefficient measurements. L. Zhang made the chromophore films and conducted the DFT calculations. Z. Zeng, J. Liu, T. Luo, Z. Li, J. Liao, L. Zhang and F. Liu wrote the manuscript and all authors discussed the experiments and final manuscript.

# Conflicts of interest

There are no conflicts to declare.

# Acknowledgements

This work was supported by the Guangzhou Municipal Science and Technology Project (No. 202102010426), the National Natural Science Foundation of China (No. 21805049) and Scientific Research Projects (YBN2020085045) of Huawei Technologies Co., Ltd. Fenggang Liu would like to thank Dr Chunngai Hui at Huawei Technologies Co., Ltd and Hui Chen at the State Key Laboratory of Optoelectronic Materials and Technology (Sun Yat Sen University) for their invaluable discussions and help in this work.

# Notes and references

1 L. R. Dalton, P. A. Sullivan and D. H. Bale, *Chem. Rev.*, 2010, **110**, 25–55.
2 J. Wu, Z. a. Li, J. Luo and A. K. Y. Jen, *J. Mater. Chem. C*, 2020, **8**, 15009–15026.
3 D. L. Elder, S. J. Benight, J. Song, B. H. Robinson and L. R. Dalton, *Chem. Mater.*, 2014, **26**, 872–874.
4 U. Koch, C. Uhl, H. Hettrich, Y. Fedoryshyn, C. Hoessbacher, W. Heni, B. Baeuerle, B. I. Bitachon, A. Josten, M. Ayata, H. Xu, D. L. Elder, L. R. Dalton, E. Mentovich, P. Bakopoulos, S. Lischke, A. Krueger, L. Zimmermann, D. Tsiokos, N. Pleros, M. Moeller and J. Leuthold, *Nat. Electron.*, 2020, **3**, 338–345.
5 L. Jiang, J. Wu, K. Chen, Y. Zheng, G. Deng, X. Zhang, Z. Li and K. S. Chiang, *Sens. Actuators, B*, 2020, 305.
6 T. Harter, C. Fuellner, J. N. Kemal, S. Ummethala, J. L. Steinmann, M. Brosi, J. L. Hesler, E. Bruendermann, A. S. Mueller, W. Freude, S. Randel and C. Koos, *Nat. Photonics*, 2020, **14**, 601–606.
7 J. Wu, W. Wang, C. Gong, Q. Li, Z. Li, G. Deng, X. Zhang, K. Chen, Y. Gong and K. S. Chiang, *J. Mater. Chem. C*, 2017, **5**, 7472–7478.
8 Y. Salamin, B. Baeuerle, W. Heni, F. C. Abrecht, A. Josten, Y. Fedoryshyn, C. Haffner, R. Bonjour, T. Watanabe, M. Burla, D. L. Elder, L. R. Dalton and J. Leuthold, *Nat. Photonics*, 2018, **12**, 749–753.
9 M. Burla, C. Hoessbacher, W. Heni, C. Haffner, Y. Fedoryshyn, D. Werner, T. Watanabe, H. Massler, D. L. Elder, L. R. Dalton and J. Leuthold, *APL Photonics*, 2019, **4**, 056106.
10 C. Kieninger, C. Fullner, H. Zwickel, Y. Kutuvantavida, J. N. Kemal, C. Eschenbaum, D. L. Elder, L. R. Dalton,

W. Freude, S. Randel and C. Koos, *Opt. Express*, 2020, **28**, 24693–24707.
11 Y. Salamin, I.-C. Benea-Chelmus, Y. Fedoryshyn, W. Heni, D. L. Elder, L. R. Dalton, J. Faist and J. Leuthold, *Nat. Commun.*, 2019, **10**, 5550.
12 I.-C. Benea-Chelmus, T. Zhu, F. F. Settembrini, C. Bonzon, E. Mavrona, D. L. Elder, W. Heni, J. Leuthold, L. R. Dalton and J. Faist, *ACS Photonics*, 2018, **5**, 1398–1403.
13 S. Ummethala, T. Harter, K. Koehnle, Z. Li, S. Muehlbrandt, Y. Kutuvantavida, J. Kemal, P. Marin-Palomo, J. Schaefer, A. Tessmann, S. K. Garlapati, A. Bacher, L. Hahn, M. Walther, T. Zwick, S. Randel, W. Freude and C. Koos, *Nat. Photonics*, 2019, **13**, 519–524.
14 A. Messner, P. A. Jud, J. Winiger, M. Eppenberger, D. Chelladurai, W. Heni, B. Baeuerle, U. Koch, P. Ma, C. Haffner, H. Xu, D. L. Elder, L. R. Dalton, J. Smajic and J. Leuthold, *Nano Lett.*, 2021, **21**, 4539–4545.
15 C. Haffner, D. Chelladurai, Y. Fedoryshyn, A. Josten, B. Baeuerle, W. Heni, T. Watanabe, T. Cui, B. Cheng, S. Saha, D. L. Elder, L. R. Dalton, A. Boltasseva, V. M. Shalaev, N. Kinsey and J. Leuthold, *Nature*, 2018, **556**, 483–486.
16 J. Wu, M. Fan, G. Deng, C. Gong, K. Chen, J. Luo, K. S. Chiang, Y.-J. Rao and Y. Gong, *Sens. Actuators, B*, 2019, 298.
17 D. L. Elder and L. R. Dalton, *Ind. Eng. Chem. Res.*, 2022, **61**, 1207–1231.
18 D. Zhang, J. Zou, W. Chen, S.-M. Yiu, M.-K. Tse, J. Luo and A. K. Y. Jen, *Chem. Mater.*, 2022, **34**, 3683–3693.
19 H. Xu, J. Liu, J. Liu, C. Yu, Z. Zhai, G. Qina and F. Liu, *Mater. Chem. Front.*, 2020, **4**, 168–175.
20 H. Zhang, Y. Tian, S. Bo, L. Xiao, Y. Ao, J. Zhang and M. Li, *J. Mater. Chem. C*, 2020, **8**, 1380–1390.
21 D. Zhang, W. Chen, J. Zou and J. Luo, *Chem. Mater.*, 2021, **33**, 3702–3711.
22 W. Liu, Z. Zeng, T. Luo, J. Liao, Z. Li, A. Rahman, S. Li, Z. Liu and F. Liu, *Dyes Pigm.*, 2022, 205.
23 F. G. Liu, Y. H. Yang, H. R. Wang, J. L. Liu, C. L. Hu, F. Y. Huo, S. H. Bo, Z. Zhen, X. H. Liu and L. Qiu, *Dyes Pigm.*, 2015, **120**, 347–356.
24 F. Liu, Z. Zeng, A. Rahman, X. Chen, Z. Liang, X. Huang, S. Zhang, H. Xu and J. Wang, *Mater. Chem. Front.*, 2021, **5**, 8341–8351.
25 X. Zang, G. Liu, Q. Li, Z. A. Li and Z. Li, *Macromolecules*, 2020, **53**, 4012–4021.
26 R.-L. Tang, S.-M. Zhou, Z.-Y. Cheng, H. Chen, L. Deng, Q. Peng and Z. Li, *CCS Chem.*, 2020, **2**, 1040–1048.
27 Z. a. Li, X. Zang, Y. Li, Q. Li and Z. Li, *Macromol. Rapid Commun.*, 2022, **43**, 2200179.
28 Q. Zeng, X. Chen, A. Rahman, Z. Zeng, Z. Liang, L. Shi, Z. Huang, S. Bo, F. Liu and J. Wang, *Mater. Chem. Front.*, 2022, **6**, 1079–1090.
29 Z. Shi, J. Luo, S. Huang, Y.-J. Cheng, T.-D. Kim, B. M. Polishak, X.-H. Zhou, Y. Tian, S.-H. Jang, D. B. Knorr Jr., R. M. Overney, T. R. Younkin and A. K. Y. Jen, *Macromolecules*, 2009, **42**, 2438–2445.
30 Z. Shi, J. Luo, S. Huang, B. M. Polishak, X.-H. Zhou, S. Liff, T. R. Younkin, B. A. Block and A. K. Y. Jen, *J. Mater. Chem.*, 2012, **22**, 951–959.
31 Z. Shi, Y.-Z. Cui, S. Huang, Z. a. Li, J. Luo and A. K. Y. Jen, *ACS Macro Lett.*, 2012, **1**, 793–796.
32 X. Zhang, M. Li, Z. Shi, R. Jin, X. Wang, Y. Yan, M. Yi, D. Zhang and Z. Cui, *J. Mater. Sci.*, 2011, **46**, 4458–4464.
33 Z. Shi, W. Liang, J. Luo, S. Huang, B. M. Polishak, X. Li, T. R. Younkin, B. A. Block and A. K. Y. Jen, *Chem. Mater.*, 2010, **22**, 5601–5608.
34 R. Wang, Z. Cheng, X. Deng, W. Zhao, Q. Li and Z. Li, *J. Mater. Chem. C*, 2020, **8**, 6380–6387.
35 C. Cabanetos, W. Bentoumi, V. Silvestre, E. Blart, Y. Pellegrin, V. Montembault, A. Barsella, K. Dorkenoo, Y. Bretonniere, C. Andraud, L. Mager, L. Fontaine and F. Odobel, *Chem. Mater.*, 2012, **24**, 1143–1157.
36 S.-H. Bae, H.-M. Kim, H. S. Min, D. Kim and T.-D. Kim, *J. Nanosci. Nanotechnol.*, 2012, **12**, 730–736.
37 F. Borbone, A. Carella, A. Roviello, M. Casalboni, F. De Matteis, G. Stracci, F. della Rovere, A. Evangelisti and M. Dispenza, *J. Phys. Chem. B*, 2011, **115**, 11993–12000.
38 Z. Shi, S. Hau, J. Luo, T.-D. Kim, N. M. Tucker, J.-W. Ka, H. Sun, A. Pyajt, L. Dalton, A. Chen and A. K. Y. Jen, *Adv. Funct. Mater.*, 2007, **17**, 2557–2563.
39 T.-D. Kim, J. Luo, J.-W. Ka, S. Hau, Y. Tian, Z. Shi, N. M. Tucker, S.-H. Jang, J.-W. Kang and A. K. Y. Jen, *Adv. Mater.*, 2006, **18**, 3038–3042.
40 H. Xu, F. Liu, D. L. Elder, L. E. Johnson, Y. de Coene, K. Clays, B. H. Robinson and L. R. Dalton, *Chem. Mater.*, 2020, **32**, 1408–1421.
41 P. A. Sullivan, H. Rommel, Y. Liao, B. C. Olbricht, A. J. P. Akelaitis, K. A. Firestone, J.-W. Kang, J. Luo, J. A. Davies, D. H. Choi, B. E. Eichinger, P. J. Reid, A. Chen, A. K. Y. Jen, B. H. Robinson and L. R. Dalton, *J. Am. Chem. Soc.*, 2007, **129**, 7523–7530.
42 S. He, Z. Liang, X. Chen, Z. Zeng, L. Shi, Z. Huang, S. Zhang, X. Geng, F. Liu and J. Wang, *Dyes Pigm.*, 2022, 203.
43 J. A. Davies, A. Elangovan, P. A. Sullivan, B. C. Olbricht, D. H. Bale, T. R. Ewy, C. M. Isborn, B. E. Eichinger, B. H. Robinson, P. J. Reid, X. Li and L. R. Dalton, *J. Am. Chem. Soc.*, 2008, **130**, 10565–10575.
44 H. Xu, D. L. Elder, L. E. Johnson, Y. de Coene, S. R. Hammond, W. Vander Ghinst, K. Clays, L. R. Dalton and B. H. Robinson, *Adv. Mater.*, 2021, 33.
45 M. J. Frisch, G. W. Trucks, H. B. Schlegel, G. E. Scuseria, M. A. Robb, J. R. Cheeseman, G. Scalmani, V. Barone, B. Mennucci, G. A. Petersson, H. Nakatsuji, M. Caricato, X. Li, H. P. Hratchian, A. F. Izmaylov, J. Bloino, G. Zheng, J. L. Sonnenberg, M. Hada, M. Ehara, K. Toyota, R. Fukuda, J. Hasegawa, M. Ishida, T. Nakajima, Y. Honda, O. Kitao, H. Nakai, T. Vreven, J. A. Montgomery Jr, J. E. Peralta, F. Ogliaro, M. J. Bearpark, J. Heyd, E. N. Brothers, K. N. Kudin, V. N. Staroverov, R. Kobayashi, J. Normand, K. Raghavachari, A. P. Rendell, J. C. Burant, S. S. Iyengar, J. Tomasi, M. Cossi, N. Rega, N. J. Millam, M. Klene, J. E. Knox, J. B. Cross, V. Bakken, C. Adamo, J. Jaramillo, R. Gomperts, R. E. Stratmann, O. Yazyev,

A. J. Austin, R. Cammi, C. Pomelli, J. W. Ochterski, R. L. Martin, K. Morokuma, V. G. Zakrzewski, G. A. Voth, P. Salvador, J. J. Dannenberg, S. Dapprich, A. D. Daniels, Ö. Farkas, J. B. Foresman, J. V. Ortiz, J. Cioslowski and D. J. Fox, *Gaussian 09*, Gaussian, Inc., Wallingford, CT, USA, 2009.

46 I. Davydenko, S. Benis, S. B. Shiring, J. Simon, R. Sharma, T. G. Allen, S.-H. Chi, Q. Zhang, Y. A. Getmanenko, T. C. Parker, J. W. Perry, J.-L. Bredas, D. J. Hagan, E. W. Van Stryland, S. Barlow and S. R. Marder, *J. Mater. Chem. C*, 2018, **6**, 3613–3620.

47 D. H. Park, C. H. Lee and W. N. Herman, *Opt. Express*, 2006, **14**, 8866–8884.

48 W. Jin, P. V. Johnston, D. L. Elder, A. F. Tillack, B. C. Olbricht, J. Song, P. J. Reid, R. Xu, B. H. Robinson and L. R. Dalton, *Appl. Phys. Lett.*, 2014, **104**, 243304.